Li−Biphenyl−1,2-Dimethoxyethane Solution: Calculation and Its Application

Na Liu, Hong Li,* Jun Jiang, Xuejie Huang, and Liquan Chen

Beijing National Laboratory for Condensed Matter Physics, Institute of Physics, Chinese Academy of Sciences, Beijing 100080, China

Received: November 17, 2005; In Final Form: April 6, 2006

Metallic lithium reacts with biphenyl in 1,2-dimethoxyethane (DME) solvent at room temperature. This reaction has been studied using density functional theory (DFT) at the B3LYP level together with the 6-311++G (d,p) basis set. From the energy results of the corresponding optimized geometries for intermediate complexes, the reaction can be interpreted as a charge-transfer process between lithium and biphenyl followed by Li^+ coordination with ether oxygens in DME. In addition, the experimentally observed vibrational bands can be unambiguously assigned and interpreted according to the normal modes calculated for the biphenyl−Li−DME complex. This organic complex solution has been demonstrated as a very effective chemical lithiation agent. V_2O_5 can be lithiated up to 1.45 lithium ions per formula. The lithiated V_2O_5 shows a high Li-extraction capacity of 173 mAh/g as cathode material for lithium ion batteries.

Introduction

It was reported in the early 1900s that alkali metal can react with certain aromatic hydrocarbons in ether solvent to form an alkali solution at room temperature.[1,2] Theoretical and experimental investigations of the reaction have been carried out, and the computational modeling of the complexes of alkali metal with aromatic compounds has received considerable attention.[3−6] However, a better understanding of the complex molecular system interactions is needed to develop potential applications for the resulting solutions. To the best of our knowledge, theoretical study on the vibrational spectroscopy of the system has not been reported so far.

On the other hand, the alkali solution, especially lithium solution, can be used in synthetic chemistry, which has found considerable applications in many fields.[7−9] Particularly, it could be used to synthesize certain Li-containing compounds that are difficult to be obtained directly. It has long been known that V_2O_5 can be inserted by 1.8 Li per formula electrochemically in a lithium cell. This corresponds to a very high Li-storage capacity of 250 mAh/g, much higher than the 140 mAh/g of $LiCoO_2$, a widely used cathode material for commercial Li ion batteries. Because of safety cautions, metal lithium cannot be used as an anode in rechargeable lithium batteries. Therefore, the cathode material should be a Li-containing compound serving as a lithium reservoir to couple with the graphite anode. Great effort has been made to prepare lithium vanadium oxide, which could be used as the Li-source cathode material. Up to now, direct synthesis has not been successful. On the other hand, chemical lithiation methods have attracted much attention. Among them, LiI/acetonitrile[10] and *n*-BuLi in hexane[11] were widely used as lithiation agents. However, the amount of extractable lithium is less than 1 mol of lithium per formula in both cases.

In this paper, in the first section, density functional theory (DFT) calculations are carried out to investigate the molecular structure and thermodynamic parameters of intermediate complexes in the reaction, and the reaction process is interpreted accordingly. The experimental vibrational bands are unambiguously assigned on the basis of the normal modes calculated for the biphenyl−Li−1,2-dimethoxyethane (DME) complex. In the second section, we demonstrate here that V_2O_5 can be lithiated up to 1.45 lithium ions per formula by a lithium biphenylide solution in DME. Nearly 1.2 lithium ions can be deintercalated in the first charge, which corresponds to a Li-extraction capacity of 173 mAh/g.

Computational Details

Standard DFT calculations at the B3LYP level have been performed with the Gaussian 98 software package.[12] The 6-311++G (d,p) basis set and Becke's three-parameter exchange functional, in combination with the Lee−Yang−Parr correlation function (B3LYP) were used in structure optimization and single-point calculation.[13] In addition, vibration frequency analysis was also performed at the same level. The optimized structure was used as input for harmonic vibration frequency calculations. The vibration modes were assigned by means of visual inspection using the Gaussview program.[14] The theoretical values of frequencies were scaled down uniformly by a factor of 0.99, as reported by Scott and Radom.[15]

Experimental Section

Sample Preparation. V_2O_5 powder and biphenyl with high purity (over 99.0%) are commercially available and were used as received. Reagent grade DME was distilled and dehydrated over molecular sieves before use. The organic complex lithium solution was prepared by dissolving 1.0 M metallic lithium in DME solvent, in the presence of equimolar biphenyl as the dissolving agent. One gram of V_2O_5 (about 50 mol % less than lithium) was immersed in the dark-green lithium solution and allowed to react for 24 h at room temperature. The resulting solution turned transparent and colorless, while the color of the solid changed from orange to black. The product was filtered, washed with DME, and then dried overnight under vacuum at room temperature to remove the remaining solvent. Since the

* Corresponding author: Tel: 0086-10-82648067. Fax: 0086-10-62556598. Address: Zhongguancun South 3rd Street No. 8, Beijing 100080, China. E-mail address: hli@aphy.iphy.ac.cn.

10.1021/jp056653p CCC: $33.50
Published on Web 05/06/2006

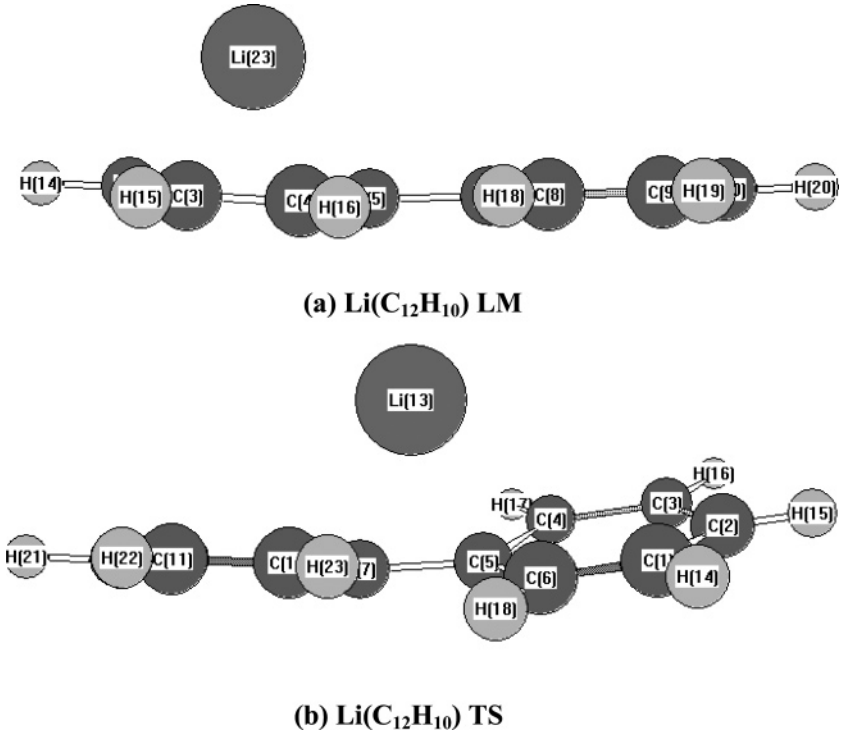

Figure 1. Drawings of the conformational structures of (a) the LM and (b) TS for $Li(C_{12}H_{10})$.

solution was sensitive to oxygen and moisture, all of the preparations were carried out in an MBRAUN Labmaster 130 glovebox filled with pure argon. For comparison, $Li_xV_2O_5$ compound was prepared in acetonitrile solution using LiI as the lithiation agent, as previously described in ref 10.

Structural and Spectral Characterization. The lithium and vanadium contents in the $Li_xV_2O_5$ samples were analyzed with inductively coupled plasma atomic emission spectrophotometry (ICP-AES). An X-ray powder diffraction study was performed with a Rigaku DMAX/2000 diffractometer. X-ray profiles were measured using a monochromatized Cu−Kα radiation source ($\lambda = 1.5418$ Å) at 40 kV and 100 mA in the 2θ range of 10−80°. The morphologies of the sample particles were examined with an XL30 S-FEG scanning electron microscope (SEM). The Fourier transform infrared (FT-IR) absorption spectra were recorded on a Bruker Vector 200 FT-IR spectrometer over the range of 4000−400 cm^{-1}. For each IR spectrum, 50 scans were recorded and averaged. The resolution was set to 2 cm^{-1}.

Electrochemical Measurement. The composite cathode for a lithium cell was prepared by blending 80 wt % active material, 15 wt % acetylene black (AB), and 5 wt % poly(vinylidene fluoride) (PVDF) dissolved in 1-methyl-2-pyrrolidone (NMP) to form a slurry. The homogeneously mixed slurry was coated on aluminum foil and dried to remove the solvent. The electrode was further dried at 120 °C under vacuum for 8 h until the residual solvent and volatile impurities were completely removed. The two-electrode cell for the electrochemical test composed of 1 M $LiPF_6$/EC+DMC (ethylene carbonate plus dimethyl carbonate in a 1:1 volume) electrolytes (Beijing Phylion Battery Company, battery grade), a cathode, a Celgard 2300 separator, and a lithium anode. The galvanostatic charge−discharge cycles were carried out with a current density of 0.156 mA cm^{-2}.

Results and Discussion

Optimized Structures. To gain a better understanding of the chemical nature of the bonding in this reaction, a theoretical study on the various possible interactions between lithium and the other two reactants was undertaken.

We first observed various stationary points for the $Li(C_{12}H_{10})$ complex, and two stationary points were found. One has the lithium atom located at the center above one of the two C_6-rings of the biphenyl. The calculated frequencies are all real, indicating a true local minimum (LM) on the potential energy surface. The aromatic system exhibits two equivalent minima, which are strictly identical. The other has the lithium atom located just between the two C_6-rings of the biphenyl. This stationary point has the sole imaginary frequency at -107 cm^{-1}, indicating a transition state (TS) between the two equal minima. The conformational structures of the complexes drawn by the use of ChemBats3D software[16] are shown in Figure 1. It can be seen that the resulting structures are nonplanar. The deviation from planarity is 16° for the TS structure of $Li(C_{12}H_{10})$. In the LM structure for $Li(C_{12}H_{10})$, the optimal distance from the lithium atom to the near center of one of the two phenyl rings is 1.67 Å. The complex favors the LM structure rather than the TS as a result of the maximized charge−quadrupole interactions.

Then, the geometry optimization of the $Li_2(C_{12}H_{10})$ complex was carried out. Two stationary points were found, as shown in Figure 2. One has the two lithium atoms on the near centers above and below the two C_6-rings of the biphenyl, respectively, while, in the other structure, the two lithium atoms bind on the same side above the rings. The optimal distances from the lithium atom to the near center of the C_6-ring are 1.63 and 1.72 Å for the two LMs, respectively.

Figure 3 illustrates the optimized structures for the Li^+−DME complex. It can be seen that the main difference between the two structures is the binding geometry of the lithium atom with the ether oxygens in DME. In the former structure, lithium lies within the plane defined by the C−O−C moiety to form a trigonal-planar geometry, while, in the latter structure, lithium binds with both oxygen atoms in DME, and the O−Li−O angle is 83°.

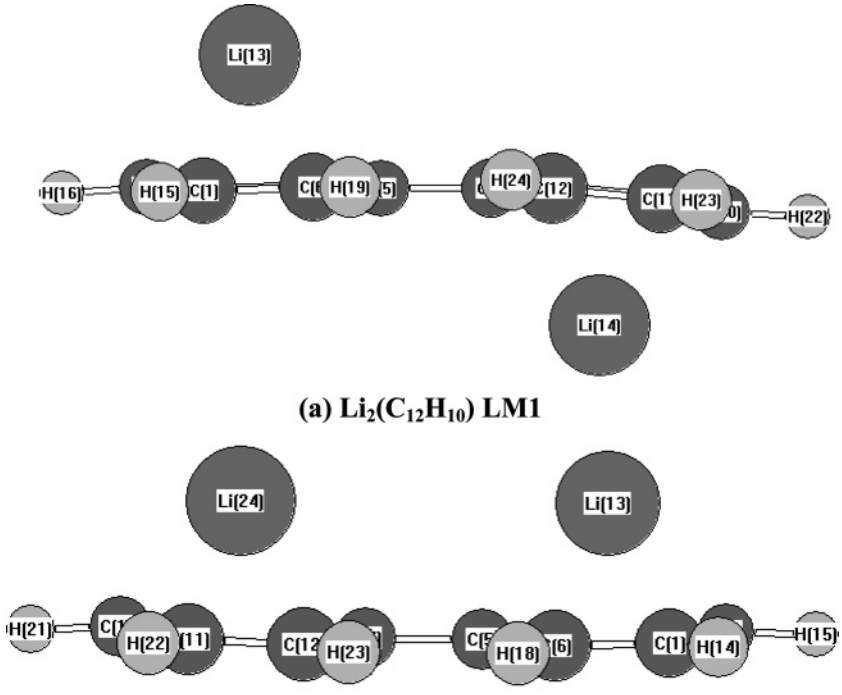

Figure 2. Drawings of the conformational structures of the two LMs (a) LM1 and (b) LM2 for $Li_2(C_{12}H_{10})$.

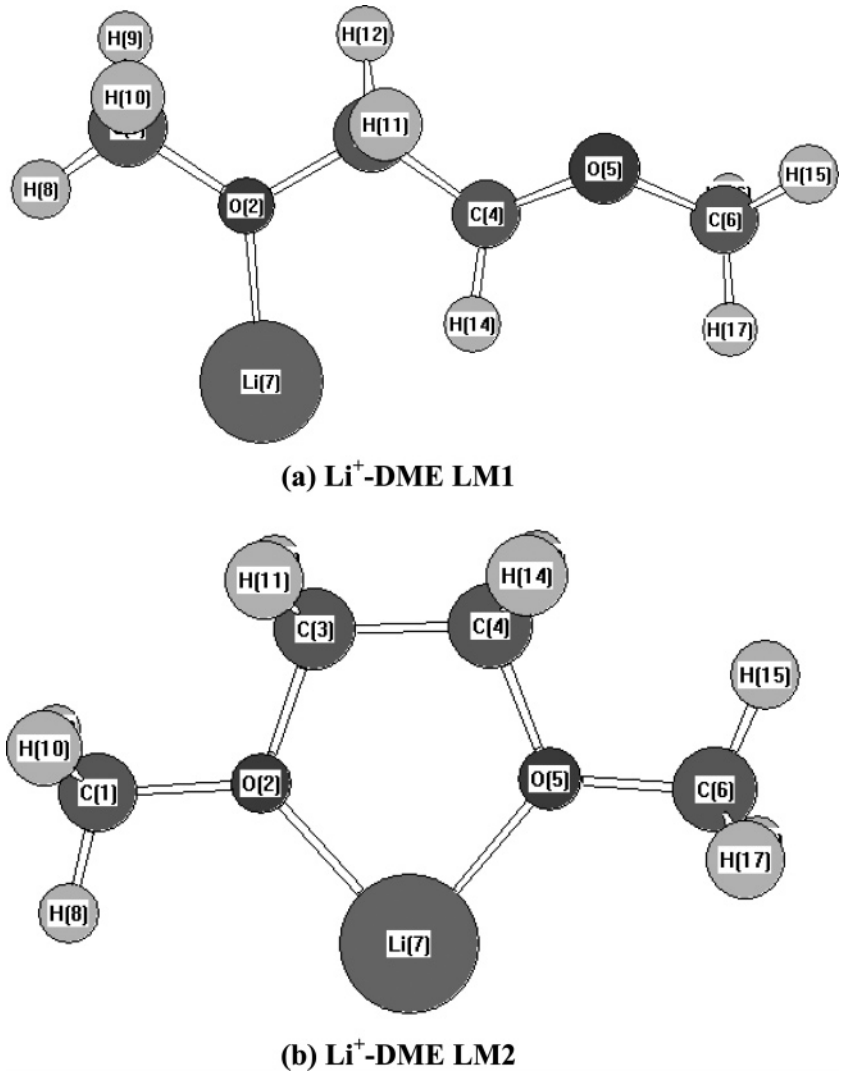

Figure 3. Optimized conformational structures (a) LM1 and (b) LM2 of the $Li^+(C_4H_{10}O_2)$ complex.

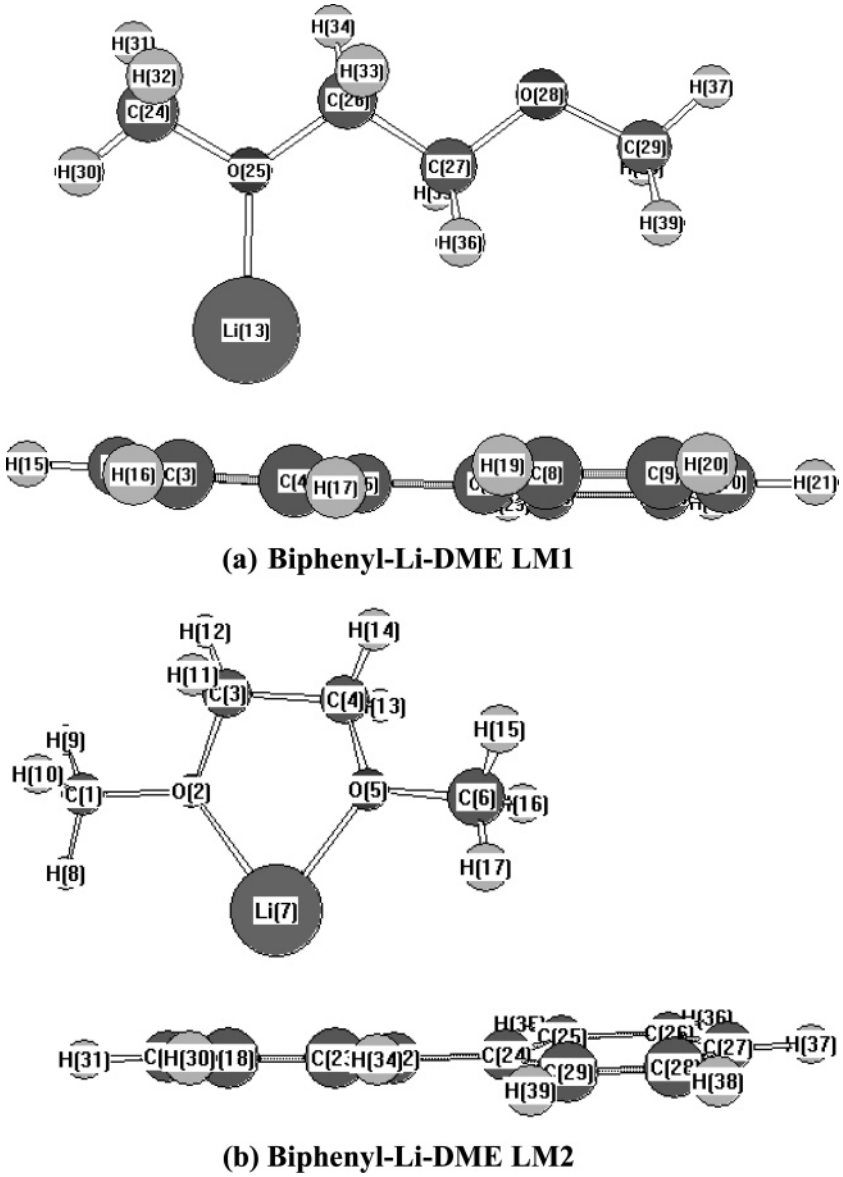

Figure 4. Optimized conformational structures (a) LM1 and (b) LM2 of the biphenyl−Li−DME complex.

In addition, the biphenyl−Li−DME complex was also taken into consideration, and two optimized geometries were obtained (see Figure 4). One has the lithium atom binding with one of the ether oxygens in DME, and the other has the lithium atom located between two oxygens, which is similar to the conformations of the Li^+−DME complex. The vertical distances between the lithium atom and the phenyl ring plane are 1.76 and 1.89 Å, respectively.

Calculated Frequencies and Energies. In Figure 5 the predicted scaled vibration frequencies for Li^+−DME (spectra c and e) and biphenyl−Li−DME (spectra d and f) with different Li−O binding geometries are compared with the experimental spectrum of 1 M lithium and biphenyl in DME (spectrum b) in the range of 400−1250 cm^{-1}. For comparison, the corresponding IR spectrum of the solution before dissolution of metallic lithium (spectrum a) is also shown in Figure 5. It can be seen that spectra a and b are quite different from each other in this region, which implies that the addition of lithium has induced the interactions of the alkali metal with the solvent as well as the arene molecules. It should be noted that a new strong band appears at 556 cm^{-1} in spectrum b after the dissolution of lithium, and the calculated IR spectrum d also revealed a strong band at the same frequency, which was assigned to a jumping

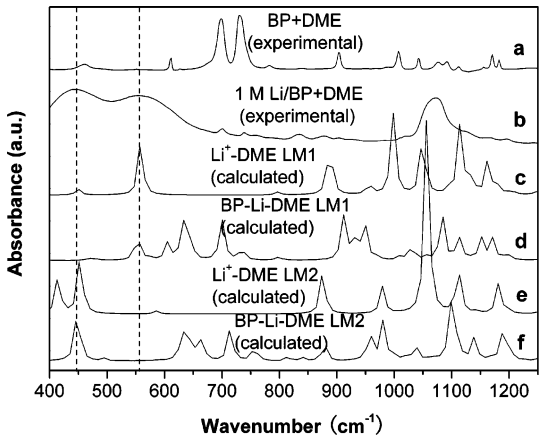

Figure 5. Recorded experimental IR spectra of 1 M biphenyl in DME solvent (a) before and (b) after the dissolution of metallic lithium; calculated IR spectra of $Li^+(C_4H_{10}O_2)$: (c) LM1 and (e) LM2; and calculated IR spectra of biphenyl−Li−DME: (d) LM1 and (f) LM2, at the B3LYP/6-311G++(d,p) level.

vibration of Li between the phenyl ring and the oxygen of DME according to the observed motion using the Gaussview software. Moreover, the band located at 460 cm^{-1} in spectrum a is

TABLE 1: Total Energies (*E*, hartrees), Zero-Point Energies (ZPEs, hartrees), and Relative Gibbs Free Energies (Δ*G*, kJ/mol) in the Different Complexes[a]

system	*E*[b]	ZPE	Δ*G*
Li	−7.491333		
Li^+	−7.284918		
$C_{12}H_{10}$	−463.238651	0.180835	
$Li(C_{12}H_{10})$ (LM)	−470.750544	0.179281	−33.2
$Li(C_{12}H_{10})$ (TS)	−470.744014	0.179787	−13.9
$Li_2(C_{12}H_{10})$ (LM1)	−478.263570	0.179985	−87.4
$Li_2(C_{12}H_{10})$ (LM2)	−478.260031	0.179690	−70.0
$(C_{12}H_{10})^-$	−463.243509	0.174939	−15.98
$(C_{12}H_{10})^{2-}$	−463.120856	0.181354	305.96
$Li(C_{12}H_{10})^-$	−470.761183	0.177588	−43.4
$Li^+(C_{12}H_{10})^-$	−470.750544	0.179281	−560.9
$C_4H_{10}O_2$	−308.814206	0.140686	
$Li^+(C_4H_{10}O_2)$ (LM1)	−316.161690	0.142759	−136.7
$Li^+(C_4H_{10}O_2)$ (LM2)	−316.101418	0.145453	−197.6

[a] The B3LYP density functional level of theory with the 6-311++G(d,p) basis sets was used. [b] These values include the corresponding ZPE correction.

broadened and shifts to the lower frequency in spectrum b after the addition of lithium to the solution. This change can also be reflected in spectrum f by the appearance of a strong band located near 450 cm^{-1}, which also results from the interaction of a lithium atom with both the biphenyl and two oxygens in DME. Besides the two bands mentioned above, the other bands in spectrum b for the resulting solution can also be unambiguously interpreted on the basis of the combination of the calculated spectra d and f. The above results indicate the coexistence of intermediate biphenyl−Li−DME complexes with two different structural conformations. Moreover, it should be noted that the two bands located at 556 and 450 cm^{-1} also respectively appear in the calculated spectra for Li^+−DME complex (spectrum c and e), which is assigned to the Li−O stretch. Therefore, the change in the IR spectrum after the dissolution of lithium can be mainly ascribed to the interaction between lithium and the ether oxygens in DME. Thus, lithium may also exist in the form of an ion chelated by DME as a result of the charge-transfer reaction.

The total energies of lithium, biphenyl, DME, and the LM and TS structures for the intermediate complexes of lithium with the other two molecules, as well as the corresponding binding energies after zero-point energy correction and relative Gibbs free energies, are summarized in Table 1. According to the energy results listed in Table 1, the reaction process can be interpreted as the following:

First, the charge-transfer reaction between metallic lithium and biphenyl occurs forming $[(BP^{\bullet-})Li^+]$ adduct, which is the most thermodynamically favorable ($\Delta G = -560.9$ kJ/mol). Then, the adduct is further stabilized by the coordination of a lithium ion with DME ($\Delta G_{LM1} = -136.7$ kJ/mol; $\Delta G_{LM2} = -197.6$ kJ/mol). Therefore, the total reaction can be described by the following equation:

$$BP + Li + C_4H_{10}O_2 \leftrightarrow [(BP^{\bullet-})Li^+](C_4H_{10}O_2) \quad (1)$$

For comparison, the other two aromatic hydrocarbons naphthalene and benzene were also considered in place of biphenyl for the theoretical study. The energy results of the three aromatic systems are compared in Table 2. It can be seen that the change in the Gibbs free energy in the reaction is negative for naphthalene, as in the case of biphenyl, while, for benzene, the change is positive, which means the reaction is infeasible in view of thermodynamics. This is also demonstrated by the experiment in that lithium cannot dissolve in the benzene−DME solution.

TABLE 2: Total Energies (*E*, hartrees), Zero-Point Energies (ZPE, hartrees), Binding Energies (BE, kJ/mol) and Relative Gibbs Free Energies (Δ*G*, kJ/mol) for Different Aromatic Systems[a]

system	*E*	ZPE	BE[b]	Δ*G*
biphenyl	−463.238651	0.180835		
biphenyl−Li	−470.750544	0.179281	53.6	−33.2
naphthalene	−385.835303	0.146841		
naphthalene−Li	−393.348335	0.145559	60.7	−34.2
benzene	−232.206822	0.100076		
benzene−Li	−239.704844	0.098514	21.3	1.9

[a] The B3LYP density functional level of theory with the 6-311++G(d,p) basis sets was used. [b] These values include the corresponding ZPE correction.

Chemical Lithiation of Vanadium Pentoxide. A lithium vanadium bronze ($Li_xV_2O_5$) was obtained by the reduction of solid V_2O_5 with the lithium solution at room temperature. The reaction can be described in the following equation:

$$V_2O_5 + x[(C_{12}H_{10})^{\bullet-}\ Li^+](C_4H_{10}O_2) \rightarrow Li_xV_2O_5 + xC_{12}H_{10} + C_4H_{10}O_2 \quad (2)$$

In this reaction, V^{5+} ions within the V_2O_5 lattice are reduced to a lower valence state, and Li^+ ions diffuse into the layered host to maintain electroneutrality. The elemental composition analysis result shows that the composition of the product is $Li_{1.45}V_2O_5$, namely, the final valence state of the vanadium is +4.41. So the compound can be simply formularized as $Li_xV_2O_5$ ($x = 1.45$). Compared to the above result, ICP analysis showed that the Li content in $Li_xV_2O_5$ was 0.94 for the sample lithiated with LiI in acetonitrile.

Figure 6 shows the powder X-ray diffraction (XRD) patterns of $Li_xV_2O_5$ samples prepared by two different lithiation agents in comparison with that of the pristine V_2O_5 phase. All of them clearly indicate the polycrystalline nature of the ingredients and a good crystallinity. But the slightly reduced intensity in the XRD diagram of the lithiated samples suggests that they are less crystalline than V_2O_5. It also can be seen that there are significant differences between them, and marked changes in the main lines are observed after the chemical intercalation of lithium ions in the host lattice of V_2O_5. Both the $Li_{0.94}V_2O_5$ and $Li_{1.45}V_2O_5$ samples have been indexed in the orthorhombic crystal system, which belongs to the *Cmcm* space group and corresponds to δ-LiV_2O_5 [JCPDS 89-4731]. The intensity of the major diffraction peak (17.95°) of δ-LiV_2O_5 [JCPDS 89-4731] is high for both samples, indicating that this phase is in

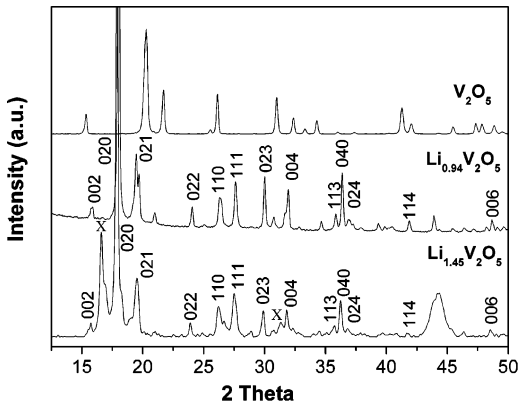

Figure 6. XRD patterns of the pristine V_2O_5 and lithiated compound $Li_xV_2O_5$ ($x = 0.94$ and 1.45) prepared by different lithiation agents. Indexed peaks correspond to the LiV_2O_5 phase, "×" indicates the γ-LiV_2O_5 phase.

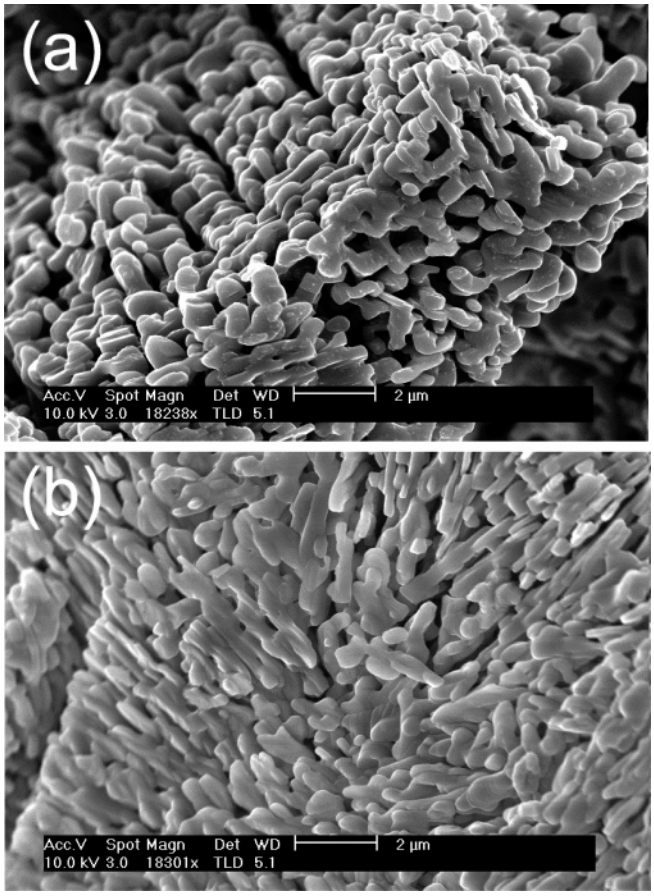

Figure 7. SEM images of vanadium pentoxide (a) before and (b) after lithiation.

majority. Moreover, other diffraction lines (noted "×" on the diagram) can be detected for the $Li_{1.45}V_2O_5$ sample and reveal the presence of another phase in this material, assigned to the γ phase of $Li_xV_2O_5$ [JCPDS 46−0102].

The SEM micrographs of vanadium pentoxide powders before and after chemical lithiation by the Li−biphenyl−DME complex solution are illustrated in Figure 7. Figure 7a is the SEM image of the raw material. It can be seen that the particles in the pristine V_2O_5 are mostly regular in form. The ellipsoidal particles whose dimensions are less than 1 μm are interconnected in the form of separated porous agglomerates, 20−40 μm in size, which may behave as a versatile host structure for the reversible intercalation of lithium ions. The morphology of the synthesized $Li_xV_2O_5$ is shown in Figure 7b. The texture of the lithiated powders is quite similar to that of the pristine one, but the arrangement of the particles is less orderly. It reveals the structural changes to a certain degree induced by the insertion of lithium ions. The decrease in crystallinity is also observed in XRD.

To characterize the electrochemical performance of the samples obtained from different lithiation agents, metallic lithium coin cells were made and tested. The cells were cycled between 2.5 and 4.0 V versus Li/Li^+ at a constant current density of 0.156 mA cm^{-2}. The first charge−discharge curves of the $Li_xV_2O_5$ samples are compared in Figure 8. The initial potentials were 3.20 and 2.64 V, respectively. It can be seen that both lithium vanadium oxides readily undergo a variety of intercalation and ion-exchange reactions. The two well-known plateaus located at 3.3 and 3.4 V, which are usually reported for the crystalline V_2O_5,[17,18] appear during the charging process. It should be noted that a plateau located at 3.6 V is observed for

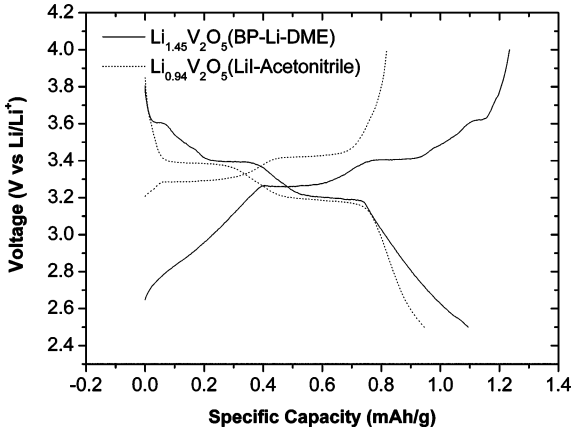

Figure 8. The first charge−discharge curves of the lithiated compound $Li_xV_2O_5$ (x = 0.94 and 1.45) at a constant current density of 0.156 mA/cm^2.

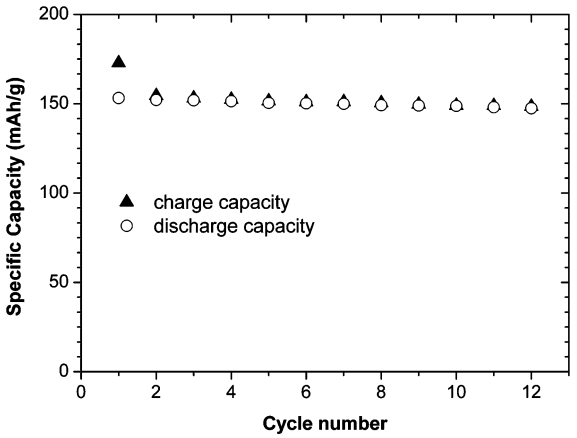

Figure 9. The cycle performance of the half-cell with the $Li_xV_2O_5$ electrode as a function of its age, performed between 2.5 and 4.0 V vs Li/Li^+ at a constant current density of 0.156 mA/cm^2.

the $Li_{1.45}V_2O_5$ sample, which reveals the presence of the γ-phase according to the results of Cocciantelli et al.[19,20] This is in agreement with the XRD results. The discharge process also contains three corresponding plateaus, and the discharge capacity is nearly the same as the charge capacity, indicating that the lithium deintercalation is reversible.

Moreover, 0.8 and 1.2 lithium ions per V_2O_5 formula are respectively deintercalated in the first charging process of $Li_{0.94}V_2O_5$ and $Li_{1.45}V_2O_5$. Garcia et al.[21] prepared $Li_xV_2O_5$ (x = 1.6) composed of the δ and γ phase with n-butyllithium in hexane. Electrochemical measurement showed that only one lithium ion per formula can be removed from the rich lithiated compound in the first charge. They ascribed this result to the chemical oxidation in air, which leads to the formation of inactive species such as Li_2CO_3 or LiOH, and the damaging presence of the puckered γ phase in large amount. In our case, we also found that lithium ions cannot be fully deintercalated during the first charge, but a more extractable lithium ion and a higher Coulombic efficiency were achieved. This could be explained by less chemical oxidation in air and the smaller amount of irreversible γ phase in the material prepared by the Li−biphenyl−DME complex solution. In addition, the cycle performance of the $Li_{1.45}V_2O_5$ sample is illustrated in Figure 9. The maintained capacity of the material is 148 mAh/g after 12 cycles. The evolution of the specific capacity of the $Li_{1.45}V_2O_5$ electrode confirms its good structural stability.

Conclusions

The theoretical structure and vibrational frequency calculations for the interaction of lithium and biphenyl in DME were performed using DFT. Optimized geometries and the corresponding energies for various intermediate complexes of lithium with biphenyl and DME molecules are obtained. From the energy results, the reaction can be interpreted as a charge-transfer process between lithium and biphenyl followed by Li^+ coordination with ether oxygens in DME. The absorption bands in the experimental IR spectrum for the resulting solution can be unambiguously assigned on the basis of the combination of the two optimized structures for the biphenyl−Li−DME complex, which indicates their coexistence. The calculated IR spectra for the Li^+−DME complex indicate that lithium may also exist in the form of an ion chelated by DME in the resulting solution.

The Li−biphenyl−DME complex solution is successfully employed as the lithiation agent for vanadium pentoxide, and this lithiation method provides the advantage of a rapid, single-step approach. Multiphased lithium vanadate was conveniently obtained at room temperature. Additionally, 1.2 lithium ions per formula (corresponding to 173 mAh/g specific capacity) can be deintercalated in the first charge. The $Li_{1.45}V_2O_5$ electrode shows good reversibility during the charge−discharge cycles (2.5−4.0 V vs Li/Li^+). The maintained capacity of the material is 148 mAh/g after 12 cycles.

Acknowledgment. The authors appreciate the financial support of the National 973 key program (2002CB211800) and the National Science of Foundation of China (Contract No. 60321001). We thank Shixuan Du and Wei Ji for help in the theoretical calculations.

References and Notes

(1) Schlenk, W.; Bergmann, E. *Justus Liebigs Ann. Chem.* **1928**, *463*, 1.

(2) Scott, N. D.; Walker, J. F.; Hansley, V. L. *J. Am. Chem. Soc.* **1936**, *58*, 2442.

(3) Irle, S.; Lischka, H. *J. Chem. Phys*. **1995**, *103*, 1508.

(4) Dorofeeva, O. V.; Moiseeva, N. F.; Yungman, V. S.; Novikov, V. P. *Thermochim. Acta* **2001**, *374*, 7.

(5) Ganguly, B.; Fuchs, B. *J. Phys. Org. Chem*. **2001**, *14*, 488.

(6) Sancho-Garcia, J. C.; Cornil, J. *J. Chem. Theory Comput*. **2005**, *1*, 581.

(7) Rieke, R. D. *Acc. Chem. Res.* **1977**, *10*, 301.

(8) Letsinger, R. L.; Finnan, J. L. *J. Am. Chem. Soc.* **1975**, *97*, 7197.

(9) Screttas, C. G.; Micha-Screttas, M. *J. Org. Chem.* **1978**, *43*, 1064.

(10) Murphy, D. W.; Christian, P. A.; Waszczak, J. V. *Inorg. Chem*. **1979**, *18*, 2800.

(11) Whiitingham, M. S.; Dines, D. B. *J. Electrochem. Soc*. **1977**, *124*, 1387.

(12) Frisch, M. J.; Trucks, G. W.; Schlegel, H. B.; Scuseria, G. E.; Robb, M. A.; Cheeseman, J. R.; Zakrzewski, V. G.; Montgomery, J. A., Jr.; Stratmann, R. E.; Burant, J. C.; Dapprich, S.; Millam, J. M.; Daniels, A. D.; Kudin, K. N.; Strain, M. C.; Farkas, O.; Tomasi, J.; Barone, V.; Cossi, M.; Cammi, R.; Mennucci, B.; Pomelli, C.; Adamo, C.; Clifford, S.; Ochterski, J.; Petersson, G. A.; Ayala, P. Y.; Cui, Q.; Morokuma, K.; Malick, D. K.; Rabuck, A. D.; Raghavachari, K.; Foresman, J. B.; Cioslowski, J.; Ortiz, J. V.; Baboul, A. G.; Stefanov, B. B.; Liu, G.; Liashenko, A.; Piskorz, P.; Komaromi, I.; Gomperts, R.; Martin, R. L.; Fox, D. J.; Keith, T.; Al-Laham, M. A.; Peng, C. Y.; Nanayakkara, A.; Gonzalez, C.; Challacombe, M.; Gill, P. M. W.; Johnson, B.; Chen, W.; Wong, M. W.; Andres, J. L.; Gonzalez, C.; Head-Gordon, M.; Replogle, E. S.; Pople, J. A. *Gaussian 98*, revision A.9; Gaussian, Inc.: Pittsburgh, PA, 1998.

(13) Becke, A. D. *J. Chem. Phys*. **1993**, *98*, 5648.

(14) Frisch, A.; Nielsen, A. B.; Holder, A. J. *GaussView Users Manual*; Gaussian Inc.: Pittsburgh, PA, 2000.

(15) Scott, A. P.; Radom, L. *J. Phys. Chem.* **1996**, *100*, 16502.

(16) *ChemBats3D*; Cambridgesoft Co.: Cambridge, MA, 1996.

(17) Pereira-Ramos, J. P.; Messina, R.; Diolet, C.; Devynck, J. *Electrochim. Acta* **1988**, *33*, 1003.

(18) Pereira-Ramos, J. P.; Messina, R.; Perichon, J. *J. Power Sources* **1985**, *16*, 193.

(19) Cocciantelli, J. M.; Menetrier, M.; Delmas, C.; Doumerc, J. P.; Pouchard, M.; Broussely, M.; Labat, J. *Solid State Ionics* **1995**, *78*, 143.

(20) Cocciantelli, J. M.; Menetrier, M.; Delmas, C.; Doumerc, J. P.; Pouchard, M.; Hagenmuller, P. *Solid State Ionics* **1992**, *50*, 99.

(21) Garcia, B.; Millet, M.; Baffier, N.; Bloch, D. *J. Power Sources* **1999**, *81*−*82*, 670.